International Journal of Engineering Research & Technology (IJERT)
ISSN: 2278-0181
Vol. 15 Issue 04 , April - 2026

Comparison Study on Solid and Beam FE Models of Strut-Based Lattice Structures under Dynamic Loads

Abdulrahman Ibrahim
Department of Mechanical Engineering
King Abdul Aziz University
Jeddah, Saudi Arabia
Mechanical and Optical Engineering
Department Strategic System Trading Co. Ltd.
(STIRA) Jeddah, Saudi Arabia

Khaled Ahmed
Department of Mechanical Engineering
King Abdul Aziz University
Jeddah, Saudi Arabia
ORCID: 0000-0003-3730-6145

Mahmoud Alzahrani
Department of Mechanical Engineering
King Abdul Aziz University
Jeddah, Saudi Arabia
ORCID: 0000-0003-4745-3368

Abstract - **This study systematically compares beam, solid, and hybrid finite element representations of six isotropic strut-based lattice topologies: BCC, Simple Cube (SC), AFCC, Iso-Truss, Octet-Truss, and FBCCXYZ under dynamic loading. The primary aim is to quantify the accuracy and limits of beam models relative to solid models as a function of strut diameter-to-length ratio (d/L%) and unit cell topology, and to establish modelling guidelines for dynamic and impact applications. Free-free modal analyses are conducted on single cells with AlSi10Mg material, three cell sizes (1, 1.5, and 3 mm), and a wide d/L% range from 2% to 48%. The 7th mode, corresponding to the first flexural mode, serves as the principal comparison metric. Mesh sensitivity studies on BCC cells, using quadratic tetrahedra for solids and BEAM188 elements for beams, determine practical convergence criteria and reveal that slenderness ratio has a stronger influence on mesh sensitivity than cell size. Relative density and infill ratio are evaluated from the cell volume and the reference cube volume, allowing assessment of mass and stiffness mismatch between models. Results show that beam models consistently underpredict natural frequencies and overpredict infill ratios, with deviations strongly dependent on both d/L% and joint connectivity. BCC exhibits minimal deviations (≈5% in frequency and ≈3% in infill at d/L% = 48%), while highly connected topologies such as Octet-Truss and FBCCXYZ reach extreme and physically inconsistent infill predictions (up to 200%) and frequency deviations exceeding 40–50%. The study demonstrates that modelling discrepancies scale with joint number and complexity, and grow rapidly with d/l%, particularly when the topology transitions from a discrete lattice to a quasi-solid morphology. The findings provide topology-specific thresholds beyond which pure beam models become unreliable and motivate hybrid modelling strategies that preserve computational efficiency while correcting joint- and geometry-dominated error sources.**

Keywords - Strut-based lattice structures, Dynamic behavior of Strut-based lattice structures, Diameter to length ratio (d/l%), Natural frequency of Strut-based lattice structures

I. INTRODUCTION

The study of lattice materials traces its roots to the broader field of cellular solids, whose foundations were laid by Gibson and Ashby in the 1980s and 1990s. Their pioneering work established the fundamental scaling relationships between density, stiffness, and strength in foams and honeycombs, framing lightweight cellular architectures as continuous analogs of naturally occurring porous materials such as wood and bone. These early theoretical frameworks provided the conceptual basis for translating natural design principles into engineered cellular materials. Building on this heritage, researchers extended cellular-solid concepts to strut-based lattices by introducing truss-like unit cells, thereby opening a route to tailor mechanical performance through deliberate modification of unit-cell geometry and topology. In a seminal contribution, Deshpande et al. developed analytical models for the octet-truss lattice that provided one of the first explicit, quantitative links between microstructural design variables and macroscopic mechanical properties, defining a paradigm for microstructure-driven performance optimization [1–5].

Advances in computational methods during the 2000s particularly finite element homogenization techniques enabled increasingly precise prediction of elastic properties and deformation behaviour in periodic lattices. These tools allowed designers to evaluate and compare candidate topologies more rigorously, moving beyond idealized analytical models toward high-fidelity numerical assessment. The rapid maturation of additive manufacturing (AM) technologies in the 2010s then transformed the field by making it possible to fabricate complex strut-based and stochastic architectures that were previously only theoretical. AM empowered engineers to realize intricate

International Journal of Engineering Research & Technology (IJERT)
ISSN: 2278-0181
Vol. 15 Issue 04 , April - 2026

lattices with controlled strut geometries, graded porosity, and tailored node morphologies, accelerating the evolution of strut-based lattices from simple beam-like cellular structures into programmable architected materials that balance structural efficiency with multifunctional requirements [4–6].

A central modelling dilemma in the analysis of these structures is the trade-off between computational efficiency and the fidelity with which local phenomena stress concentrations, joint behaviour, and plasticity are captured. Beam (line-based) element models are attractive for large-scale simulations because they are computationally inexpensive and can effectively reproduce global stiffness trends and deformation modes, especially when struts are slender and constitutive models account for AM-specific material behaviour. However, beam representations often oversimplify junctions and cannot reliably capture local nonlinearities or the additional material volume present at nodes. Solid (3D) element models, by contrast, resolve joint geometry and local stress fields much more accurately but at substantially higher computational cost. Consequently, for engineering tasks that demand many iterations such as topology optimization or exploratory parametric studies beam models are frequently used as a pragmatic, expedient choice, provided their limitations are understood [7–10].

Quantitative assessments show the limits of beam approximations: when the diameter-to-length ratio (d/l%) of struts remains below roughly 0.1, beam elements generally provide reliable predictions. Beyond this threshold, beam-based estimates of mechanical properties can deviate substantially often by more than 20% from those produced by solid 3D meshes, with the error typically increasing approximately linearly with d/l%. Alomar and Concli further observed that beam models may still be acceptable for higher d/l% ratios if deformations remain small, but accuracy deteriorates under large deformations and complex failure modes [6,11,12]. The situation is exacerbated under large plastic strains or dynamic loading: while some enhanced beam formulations and advanced constitutive laws (e.g., super-elastic or rate-dependent models) can reproduce smooth stress–strain responses and certain large-deformation behaviours, many beam models struggle to converge and to represent localized yielding, buckling, and fracture accurately. Solid models capture these nonlinearities more faithfully, but their computational expense restricts their routine use in extensive design studies [7,10,13–19].

Efforts to bridge the gap between computational efficiency and geometric fidelity have produced hybrid strategies. Luxner et al. compared plain beam, adapted beam, and continuum models and showed that plain beam models can capture global stiffness trends but underpredict stiffness at vertices because they neglect the extra material and constraint effects intrinsic to strut intersections. Their adaptation approach filling joint regions with bulk elements to mimic rigid node behaviour improved accuracy for unit cells with four or more struts meeting at a node (e.g., BCC, BCCZ, SC) but tended to over-stiffen three-strut nodes such as those in Gyroid-like architectures [20]. Tahmasebimoradi et al. extended this comparison to BCC and BCCZ lattices and reported that hybrid models required only about half the computational resources of full solid models; they also found that the effect of junction size on hybrid-model accuracy is topology-dependent, being negligible for BCCZ but significant for BCC [7,21,22]. Such studies highlight that the efficacy of joint-adaptation strategies depends strongly on local connectivity and topology.

Experimental and numerical comparisons further underscore topology- and scale-dependent behaviour. Maconachie et al. modelled a range of topologies (BCC, BCCZ, FCC, FCCZ, FBCCZ) using two-node linear beam elements and found that while beam models reproduced overall deformation modes, stiffness hierarchies, and failure mechanisms, they were less accurate at representing localized node compliance, strut misalignment, and layer-specific deformation features that often dominate real-world performance. Their tests (5 × 5 × 5 cell specimens, AlSi10Mg, cell size 7.5 mm, strut diameter 1 mm, relative densities ≈7–16 %) illustrated that line-based elements can capture global behaviour but tend to overestimate local stiffness where geometric imperfections are important. Several other studies corroborate sizeable quantitative discrepancies: beam-element simulations have been reported to diverge from experiments by errors approaching 50% in some cases [23,24]. Ruiz de Galarreta et al. explored modified beam models with increased joint diameters (+20% and +40%) and observed only marginal stiffness and yield-strength gains compared with uniform-diameter beam models; by contrast, full 3D solid models more realistically captured joint effects and the associated mechanical response [25,26].

Dynamic behaviour and modal characteristics bring further complexity: topology, relative density, and detailed mass distribution control natural frequencies and mode shapes, and joint modelling has nontrivial consequences for these dynamic properties. Syam et al. compared six strut-based topologies at 22% relative density and found tetrahedron-based structures produced the highest first-mode natural frequency in impact testing, though their use of small 2×2 specimens may have imposed boundary effects; larger 3×3 specimens would better isolate the intrinsic dynamic response of the lattice. For Kelvin lattices, Wei et al. showed that increasing relative density raises the first natural frequency, while increasing strut diameter at fixed relative density tends to lower it an inverse effect reflecting changes in mass distribution and stiffness an observation echoed by Hussain et al., who embedded octet-truss cores in gas turbine blades and reported the highest first-mode frequency for the smallest strut diameter studied (0.25 mm) due to an improved stiffness-to-mass ratio and shifted resonance [46–48].

International Journal of Engineering Research & Technology (IJERT)
ISSN: 2278-0181
Vol. 15 Issue 04 , April - 2026

Mesh and element formulation choices are likewise critical for solid-model accuracy and efficiency. Kim et al. compared linear and quadratic brick elements and found that first-order (linear) bricks provided accuracy within about 5% while offering substantially better computational performance when at least four element layers spanned the strut thickness. Their mesh-sensitivity study, which explored element sizes from 0.15 mm to 1 mm (≈6%–17% of strut diameter), showed numerical convergence for stiffness predictions below roughly 8% of the strut diameter, implying that element formulation and an ~8% mesh-size rule can balance precision and cost in many cases [49,50].

Despite extensive prior work, important gaps remain. Most comparative studies concentrate on a narrow range of topologies or geometric parameters, making it difficult to generalize model-selection guidelines across the diverse family of strut-based lattices. In particular, systematic investigations of how modelling accuracy varies with diameter-to-length ratio across different topologies are scarce. Moreover, while dynamic behaviour is crucial for many practical applications, comparative assessments of beam, solid, and hybrid modelling approaches have largely focused on static response; the influence of joint representation on mass distribution, natural frequencies, and mode shapes has not been thoroughly examined across a broad set of lattice configurations and geometrical parameters. This paper addresses these gaps by comparing solid and beam finite-element models for six isotropic strut-based unit cells BCC, SC, AFCC, Iso-Truss, Octet truss, and FBCCXYZ under dynamic loading, with the goal of establishing clearer guidelines for model selection as a function of topology, geometry, and loading regime.

The objectives of this work are to systematically quantify the accuracy and limits of beam and solid finite element models across six isotropic strut-based topologies (BCC, SC, AFCC, Iso-Truss, Octet, and FBCCXYZ) as a function of geometric parameters particularly the diameter-to-length ratio. Specifically, we aim to

1. Map deviations in predicted natural frequencies, and mode shapes between beam and solid representations over a broad d/l% range.
2. Evaluate how joint representation and node geometry affect model accuracy and the conditions under which beam models fail to capture local effects.
3. Assess mesh and element formulation sensitivities for solid models to establish practical convergence criteria.
4. Synthesize these results into topology-specific guidelines for selecting an appropriate modelling approach for dynamic and impact applications.

II. METHODOLOGY

This section outlines the research methodology adopted to address the study objectives stated in the introduction. The first section covered the trade-off between the computational efficiency and the accuracy of the results by conducting an unconstrained modal test on beam, solid, and hybrid models. Fig. 1 shows the configurations studied under dynamic loadings.

To overcome any discrepancy in the boundary conditions a free-free (unconstrained) modal test was conducted on each cell with the cell size and the slenderness ratio as controlled parameters through the tests. The configuration and their naming were inspired by the review done by Benedetti et al. [51]

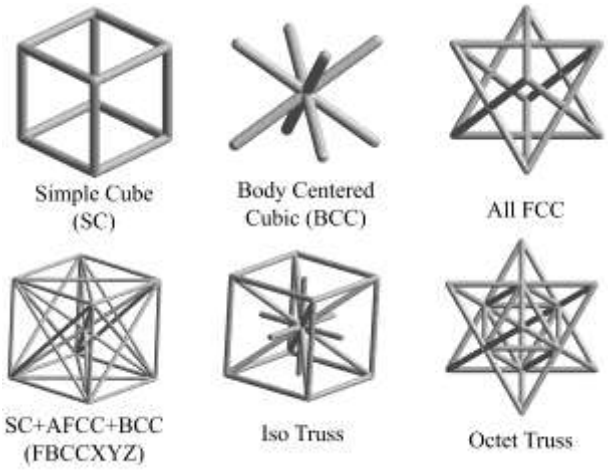

FIG. 1. **CELLS CONFIGURATIONS STUDIED**

Initially three configurations were modeled in three cell sizes (1 mm, 1.5 mm, 3 mm) with a slenderness ratio *d/l* varying from 0.02 to 0.3 with AlSi10Mg as an assigned material, to observe the Cell size effect on the dynamic behavior. For simplicity and consistency, the mechanical properties of AlSi10Mg were adopted directly from the ANSYS material library, where predefined values were used for all simulations.

In the unconstrained modal analysis, the first six modes represent the rigid body modes, while the seventh mode represents the first flexural (actual) mode. Hence the seventh mode will be considered as an evaluation criterion among the beam, solid and hybrid models. [4]

The relative density of each configuration was calculated to monitor how the error in relative density affected the natural frequency and the mode shape, the following equation was used to calculate the relative density:

$$\rho_{RD} = (V_C/(L+2\times r)^3)\times 100$$

Where "ρ_{RD}" is the relative density of the cell, "V_C" is the volume of the cell, "L" is the length of the cell, and "r" is the radius of the strut.

In the present analysis, several idealizations were introduced to streamline the investigation and emphasize the fundamental dynamic characteristics of the structure:

1- The influence of material and structural damping was disregarded, and any deviations arising from

International Journal of Engineering Research & Technology (IJERT)
ISSN: 2278-0181
Vol. 15 Issue 04 , April - 2026

manufacturing processes or geometric imperfections were omitted.

2- The material was considered to exhibit homogeneous and isotropic behavior with spatially uniform properties.

Thermal effects, including temperature variations and the associated thermal stresses, were neglected, as their contribution to the system's response was deemed insignificant within the defined scope of this study.

A mesh sensitivity analysis was conducted to determine the influence of mesh density on the accuracy and stability of the simulation results. The mesh study aimed to identify an optimal balance between computational cost and solution accuracy by comparing results across multiple mesh densities. Two comprehensive mesh studies were conducted on the BCC structure to study the effect of the cell size and the slenderness ratio on both the natural frequency and the solving time. Both studies were applied using Free-Free modal analysis.

In the first study, BCC was tested with three cell sizes (1.5 mm, 3 mm, 6 mm) at a constant slenderness ratio ($d/l\%$ = 0.1). Fig. 2 shows how the number of divisions effect the meshing of a strut diameter cross section, where the left side represent a visualization of the number of divisions for a strut circumference (8 divisions, 16 divisions, 24 divisions). In the second study, the cell size was constant while the cell slenderness ratio was tested across three values ($d/l\%$ = 0.1, 0.3, 0.5). The element type used is quadratic tetrahedron elements to avoid numerical artifacts by stiffening the model if linear elements were used. For the beam model an element type of BEAM188 was used which is based on Timoshenko beam theory. [52]

An element quality was monitored through the runs to ensure a higher value than 0.3. All simulations were conducted on a workstation equipped with an AMD Ryzen Thread-ripper PRO 3995WX 64-core processor running at 4.0 GHz and 256 GB of RAM.

Fig. 2 show the output of the two studies, where the optimum combination of accuracy and solving time appeared to be at 14 and 16 divisions. The results indicate that the slenderness ratio has a more significant influence on mesh sensitivity than cell size. This is because the slender ratio directly affects the structural stiffness and bending behaviors of each strut, making slender members more sensitive to mesh refinement. In contrast, changing the cell size primarily scales the geometry without significantly altering the deformation mode, resulting in a much smaller effect on mesh sensitivity. The finite element models using beam and solid elements of all investigated strut-based lattice cells are listed in Table 1. At d/L% of 20%.

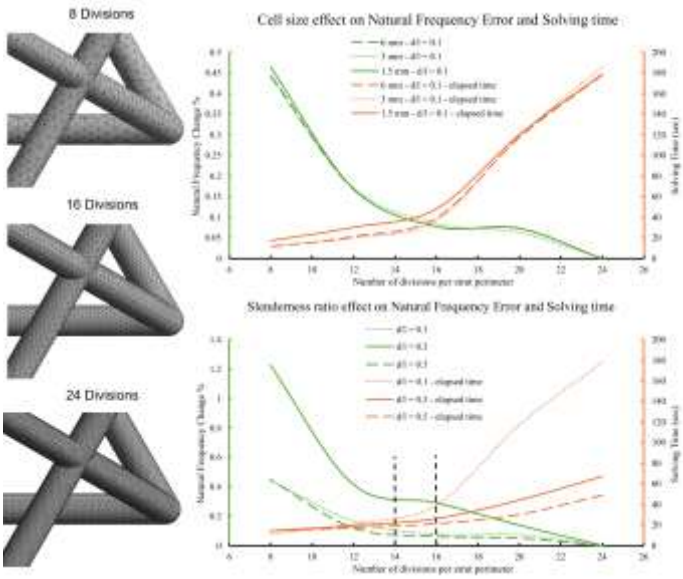

FIG. 2. **MESH SENSITIVITY ANALYSIS**

TABLE 1 MESHING OF THE SOLID AND BEAM MODELS OF THE STUDIED CONFIGURATIONS

	BCC	Simple Cube	AFCC
Solid			
Beam			
	ISO Truss	Octet Truss	FBCCXYZ
Solid			
Beam			

Altamimi et al. showed that the deformation mode of a lattice configuration is not fixed but depends on the type and direction of loading. Using FE-based G-A fits for uniaxial, shear and hydrostatic loading, they determined the stretching or bending dominated character separately for each effective property and found that many topologies switch between stretching, bending,

International Journal of Engineering Research & Technology (IJERT)
ISSN: 2278-0181
Vol. 15 Issue 04 , April - 2026

or mixed dominated behaviour when the loading mode changes. [16]

Fig. 3 illustrates the cell size study performed on the BCC, Iso-Truss, and FBCCXYZ lattice configurations to evaluate the influence of unit cell dimensions on their dynamic behaviour. The selected configurations exhibit a wide variation in strut density, allowing the effect of structural complexity to be systematically examined. The BCC configuration represents a low strut-count lattice, the FBCCXYZ configuration corresponds to a high strut-count lattice, while the Iso-Truss configuration provides an intermediate strut density. For each configuration, unit cell sizes of 1, 1.5, and 3 mm were investigated to assess the sensitivity of dynamic response to cell size across different lattice topologies.

Fig. 3 shows that slenderness ratio changes the structural stiffness, unlike the cell size which scales the stiffness uniformly. The stiffness of each strut is strongly dependent on diameter:

$$EI \propto d^4$$

A small change in diameter causes a large change in bending stiffness, which directly affects the natural frequency and the deformation mode. While changing the cell size does NOT change the deformation mode. [58-61]

If the diameter–length ratio stays the same, changing cell size:

- Preserves geometric proportions: The cell keeps the same shape; only the overall size changes.
- Scales mass and stiffness similarly: When the cell is scaled up or down, both mass and stiffness change in a predictable way, so the frequency mainly shifts due to size not a change in topology.

The following explains how mass, bending stiffness, axial stiffness, and natural frequency scales by "x":

[1] Mass

$$m = \rho V$$

Where m is the mass, ρ is the density, and V is the volume [59].

$$V' = x^3 V \rightarrow m' = \rho V' = \rho(x^3 V) = x^3 m$$

Where V' is the scaled volume by the value of x, and m' is the scaled mass.

Resulting to:

$$m \propto x^3$$

[2] Natural frequency

$$f \propto sqrt(k/m)$$

Where f is the natural frequency, k is the stiffness, and m is the mass [79].

$$k \propto x \;\&\; m \propto x^3 \rightarrow f' \propto sqrt\,(x/x^3) = sqrt\,(1/x^2) = 1/x$$

Resulting to:

$$f \propto 1/x$$

The verification of natural frequency scaling can be seen clearly through Fig. 3 especially with the 1 mm and 3 mm cells, where at any value of $d/l\%$ the natural frequency of the 1 mm cell is three times the natural frequency of the 3 mm cell of the same configuration.

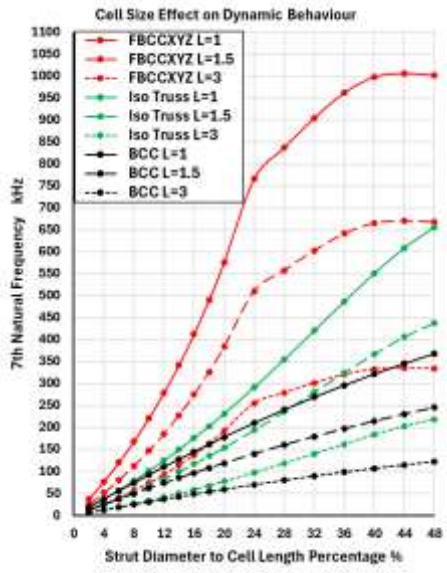

FIG. 3. CELL SIZE EFFECT ON DYNAMIC BEHAVIOR, FOR FBCCXYZ, ISO TRUSS, AND BCC

III. RESULTS

The comparison between beam element modeling and solid element modeling is made through modal analysis of unconstraint cell to avoid the effects of the boundary conditions on the achieved results. The comparison is based on the 7th mode which is the first flexural mode of the unconstrained cell. Also the infill ratio is compared for both models by comparing the elements volume to the occupying cube volume which is $(L+2r)^3$. Three cell sizes are examined; 1mm, 1.5mm, and 3mm with wide range of d/L% ratios from 2% to 48%.

The results show that the three cells BCC, SC, and AFCC, are less denes cells as shown in Fig. 4 and the other three cells; Iso and Octet Trusses and the FBCCXYZ are highly dense cells as shown in Fig. 5. In all results, beam element models show lower 7th mode natural frequencies that that of the solid model at the same d/l% ratios. On the other hand, the beam element models show higher infill ratio than that of the solid models at the same d/L% ratios. Furthermore, all investigated cells show the same exact deviations between the beam element and the solid element for all investigated sizes at the same d/L%. This result confirms the dependency of the deviations between beam and solid models on the d/L% ratios and the cell configuration. The BCC cell, Fig. 4a., has the least deviation in both the infill ratio and the 7th model natural frequency among all investigated cells. The infill maximum deviation is about 3% and the maximum frequency deviation is 5% at d/L% of 48%.

International Journal of Engineering Research & Technology (IJERT)
ISSN: 2278-0181
Vol. 15 Issue 04 , April - 2026

Due to the fact that the BCC cell has only one point of intersection with 8 members at its CG making16 joints, at this level of d/L% the infill ratio of the BCC cell is quite low, it is 38%. As shown in Fig. 5 the natural frequency of the cell decreases with the increase of the cell size. However, the deviation in the frequency and in the infilling ratio increase with the increase of the strut diameter to the cell length ratio only.

The SC cell, Fig. 4b., shows similar frequencies like the BCC cell but with quite noticeable deviations between the solid element model and the beam element model. The maximum frequency deviation is 32% at d/L% of 48%. Due to the fact that the SC cell has 8 corner intersections with three struts at each intersection making 24 joints, at this size of the strut diameter to the cell size, the solid model shows infilling ratio of 57% while the beam model shows 67% infilling ratio with 18% deviation from the solid model.

The AFCC cell, Fig. 4c., shows slightly higher frequencies and slightly higher infilling ratio than SC and BCC cells for same d/L%. The obtained deviations between the solid element model and the beam element model is higher than that of SC and BCC cells as well. The maximum frequency deviation is 45% at d/L% of 48%. Due to the fact that the AFCC cell has 8 corner intersections each with 3 struts and 6 face intersections each with four struts making 48 joints in total, at this size of the strut diameter to the cell size, the solid model shows infilling ratio of 67% while the beam model shows 97% infilling ratio with 45% deviation from the solid model.

The Iso-Truss cell, Fig. 5a., shows unified increase of the natural frequency as the d/l% increases showing frequencies slightly higher than that of the SC and slightly lower than that of the AFCC at the same d/l%. The obtained frequency deviation of the beam model from the solid model is similar to that obtained with AFCC cell and is higher than that of SC and BCC cells. The maximum frequency deviation is 45% at d/L% of 48%. Due to the fact that the Iso-Truss cell has 8 corner intersections each with 4 struts and 1 intersections at the cell CG with fourteen struts making 52 joints in total, at this size of the strut diameter to the cell size, the solid model shows infilling ratio of 75% while the beam model shows illogic 118% infilling ratio with 64% deviation from the solid model.

The Octet-Truss cell, Fig. 5b., shows three different rates of the natural frequency changes as the d/l% increases. Up to d/L% of 8% the increasing rate is very high for both solid and beam models. The frequency increase using the solid model is then slightly reduced up to d/L% of 40%, then it decreases slightly, showing frequencies significantly higher than that of the previously presented cells at the same d/l%. On the other hand, the frequency increase using the beam model kept with the same increasing rate from d/l% of 8% up to the d/L% of 48%. The obtained frequency deviation of the beam model from the solid model is similar to that obtained with Iso-Truss cell up to d/L% of 40% then it slightly decreases to 35% at d/L% of 48%. Due to the fact that the Octet-Truss cell has 8 corner intersections each with 3 struts and 6 face intersections each with eight struts making 72 joints in total, at this size of the strut diameter to the cell size 48%, the solid model shows infilling ratio of 72% while the beam model shows illogic 144% infilling ratio with 100% deviation from the solid model.

The FBCCXYZ cell, Fig 5c., shows also three different rates of the natural frequency changes as the d/l% increases. Up to d/L% of 24% the increasing rate is very high for solid model then it is slightly reduced up to d/L% of 40%, showing similar frequencies of the Octet-Truss cell. Contrary to the Octet-Truss cell, the frequencies saturated at the maximum level up to the maximum d/L% of 48%. On the other hand, the frequency increase using the beam model kept with a unified increasing rate with slight higher frequencies than that obtained with Octet-Truss cell. The obtained frequency deviation of the beam model from the solid model is significantly higher than that obtained with Octet-Truss cell up to d/L% of 24% showing 51% deviation, then it is reduced to 42% deviation at d/L% of 48%. Due to the fact that the FBCCXYZ cell has 8 corner intersections each with 7 struts, 6 face intersections each with four strutoks, and one point of intersection with 8 members at its CG making 88 joints in total, at this size of the strut diameter to the cell size 48%, the solid model shows infilling ratio of 90% while the beam model shows illogic 200% infilling ratio with 120% deviation from the solid model.

It is clear evidence as shown in Fig. 6, that the predicted infill ratio, using a beam model, deviates significantly from that created by solid model with the increase of the d/L% and the number of the joint in the cell. Due to the high connectivity and high strut density in the cell with high number of joints like the Octet-Truss and FBCCXYZ cells, the cell switch to be a solid cell with few voids rather than a strut-based lattice structure at small ratios of d/L%. The Octet-Truss switches to this dense case at d/L% of 36%, and the FBCCXYZ switches to this dense case at d/L% of 24%.

The effect of the struts interconnection in the lattice cell gets clearer and worth considering when using multiple cells. As shown in these results the beam model of the BCC cell is the least deviating model either in predicting the infill ratio or predicting the cell dynamic response as one cell. A proof-of-concept beam model of two and three cells of BCC cell is compared to similar solid model, as shown in Table 2, to evaluate the effect of the interconnection joints on the predicted results.

The single BCC cell has 8 joints as mentioned above, which contributed to 3% in fill ratio and 5% in frequency deviations of the beam model from the solid model at d/L% of 48% as shown in Fig. 7. The 2x2 configuration of BCC cell has 120 joints that contributed to the significant increase of the infill ratio from 3% to 40% at d/L% of 48%. In the same hand these joints contributed to increase the frequency deviation of the beam model from 3.5% to 26% at d/L% of 32%. Then this 2x2 configuration shows saturated deviation at 26% up to the maximum studied d/L% of 48%. Similarly, the 3x3 configuration BCC cell has 424 joints that contributed to another increase of the infill ratio to 53% at d/L% of 48%. In the same hand these joints contributed to increase the frequency deviation of the beam model to 46% at d/L% of 36%. Then this 3x3 configuration shows slightly decrease in the frequency deviation to 44% at the maximum studied d/L% of 48%.

International Journal of Engineering Research & Technology (IJERT)
ISSN: 2278-0181
Vol. 15 Issue 04 , April - 2026

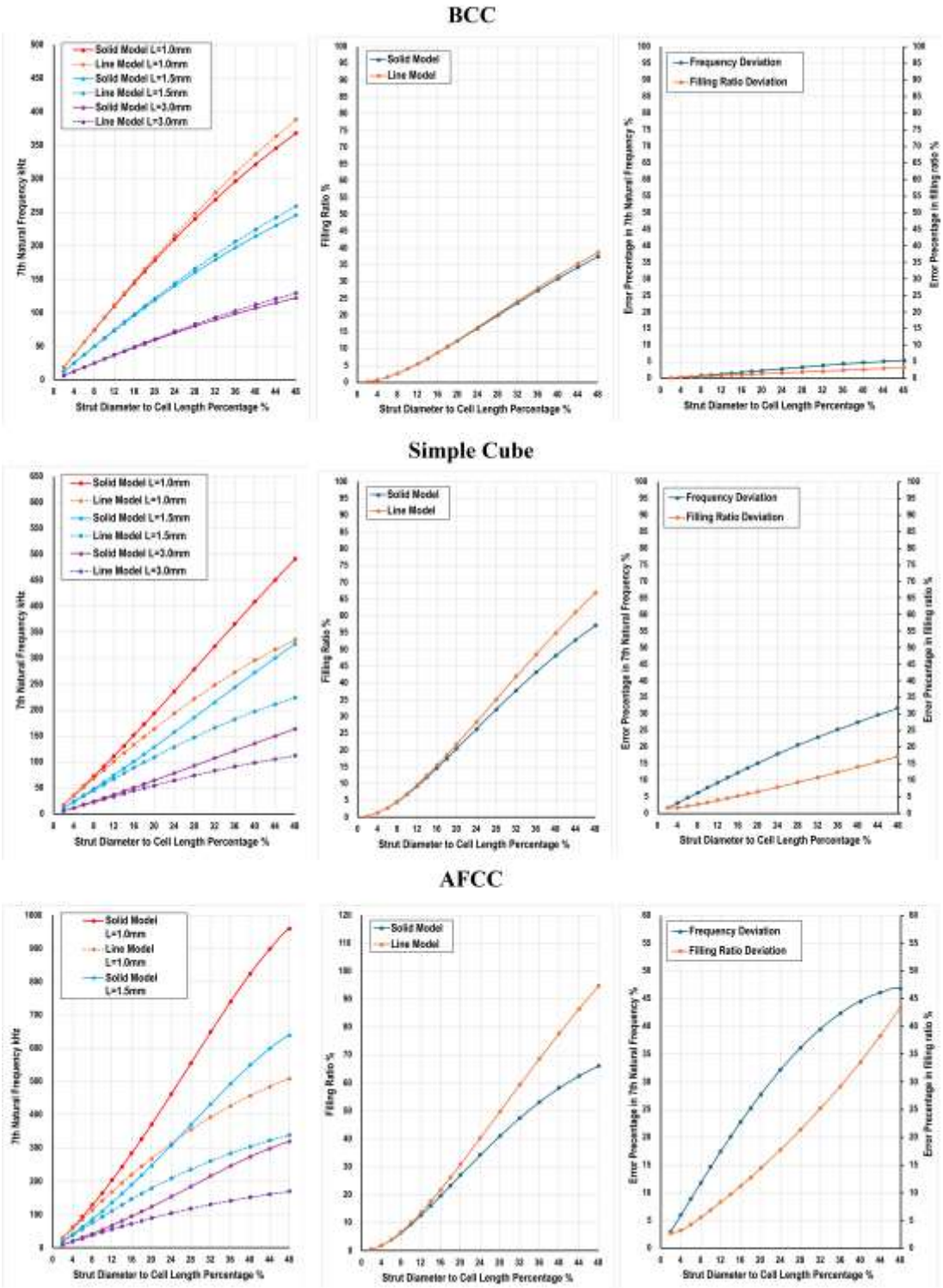

FIG. 4. ACHIEVED RESULTS FOR LESS DENS LATTICE CELLS (A) BCC, (B) SC, AND (C) AFCC CELLS

International Journal of Engineering Research & Technology (IJERT)
ISSN: 2278-0181
Vol. 15 Issue 04 , April - 2026

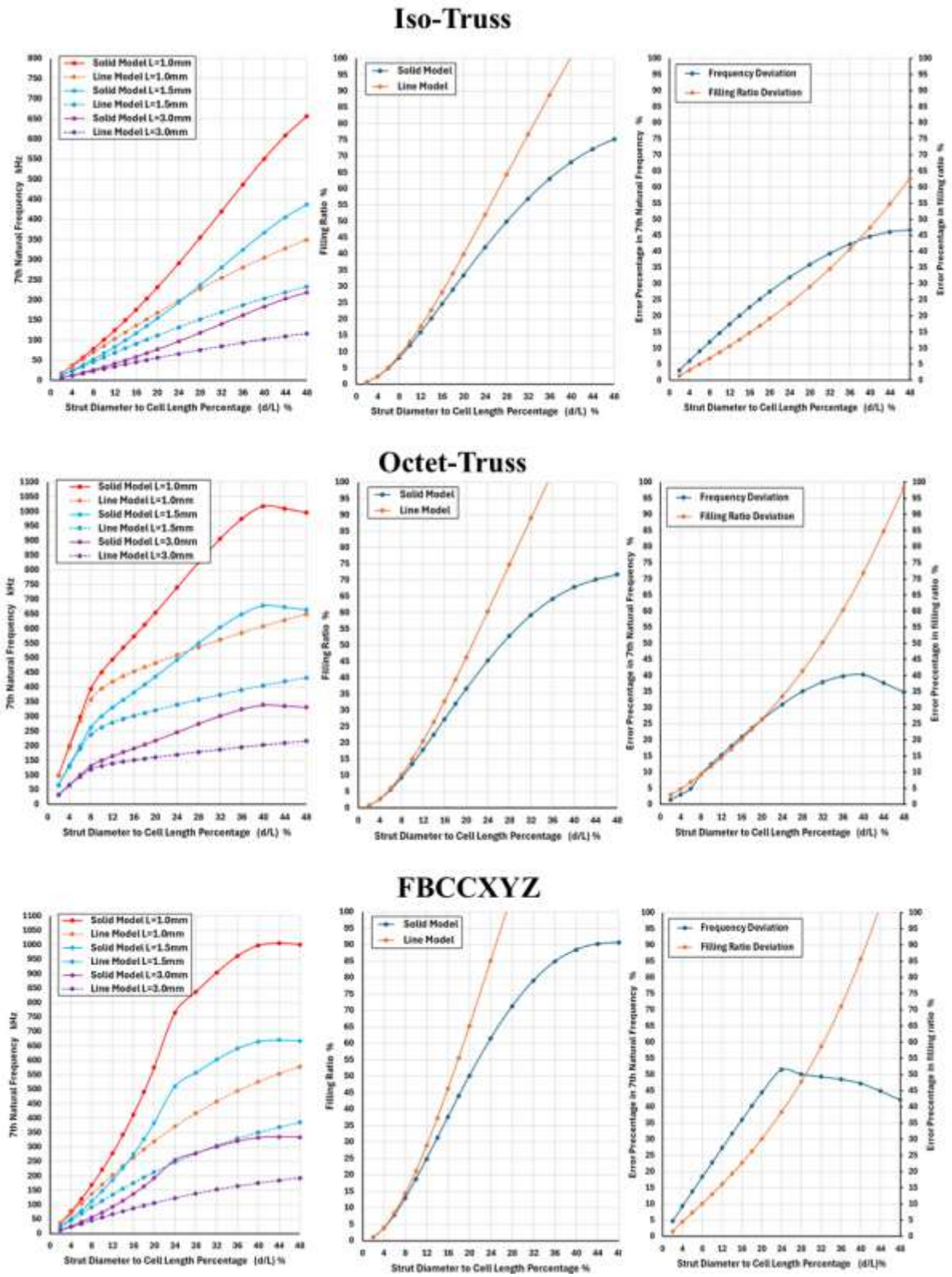

FIG. 5. ACHIEVED RESULTS FOR HIGH DENS LATTICE CELLS (A) ISO-TRUSS, (B) OCTET-TRUSS, AND (C) FBCCXYZ CELLS

International Journal of Engineering Research & Technology (IJERT)
ISSN: 2278-0181
Vol. 15 Issue 04 , April - 2026

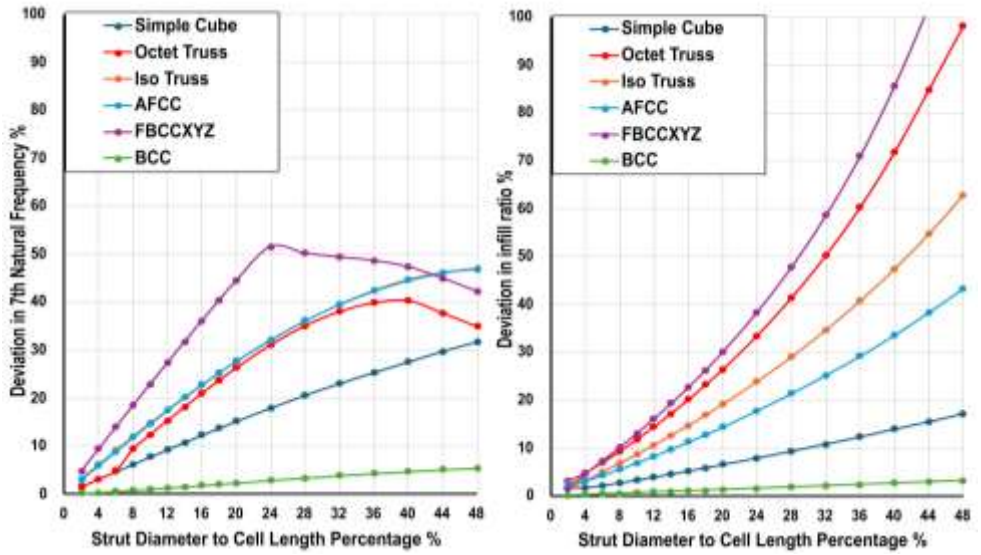

FIG. 6. DEVIATION IN FREQUENCY AND FILLING RATIO BETWEEN BEAM AND SOLID MODELS

TABLE 2 STUDIED BEAM AND SOLID MODELS OF 1X1, 2X2, AND 3X3 BCC CELLS

	Single BCC cell (8 Joints)	2x2 Configuration of BCC cell (120 joints)	3x3 Configuration of BCC cell (424 joints)
Beam Model	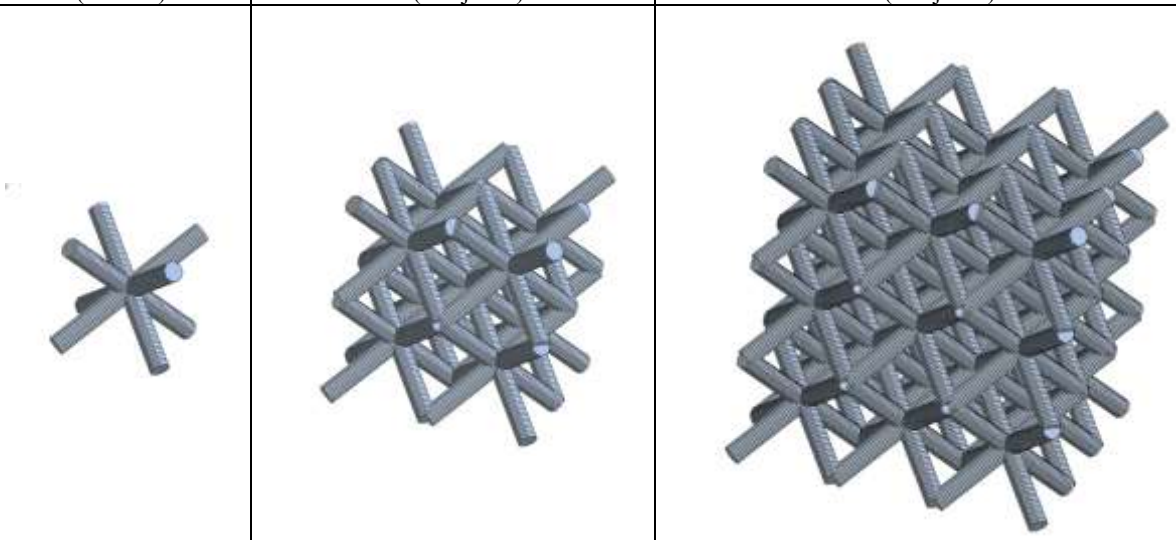		
Solid Model	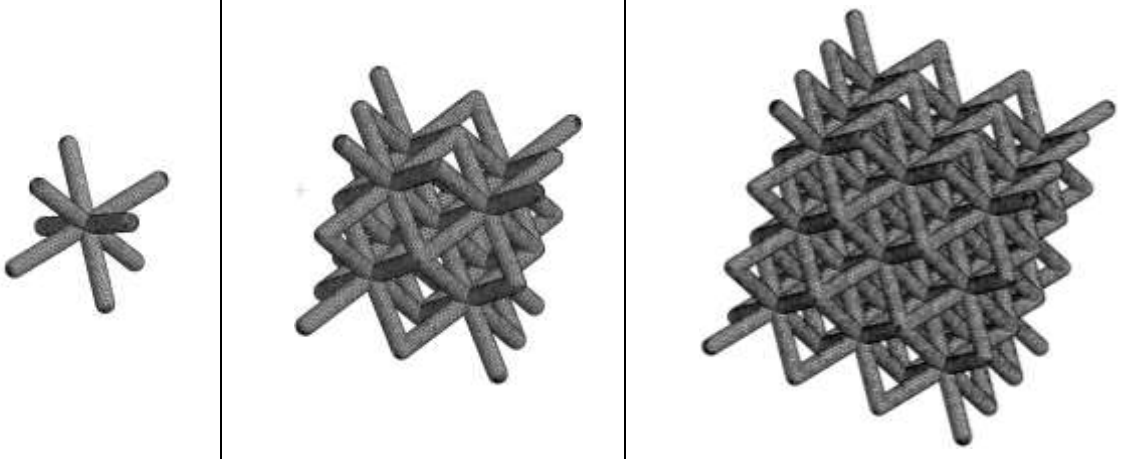		

International Journal of Engineering Research & Technology (IJERT)
ISSN: 2278-0181
Vol. 15 Issue 04 , April - 2026

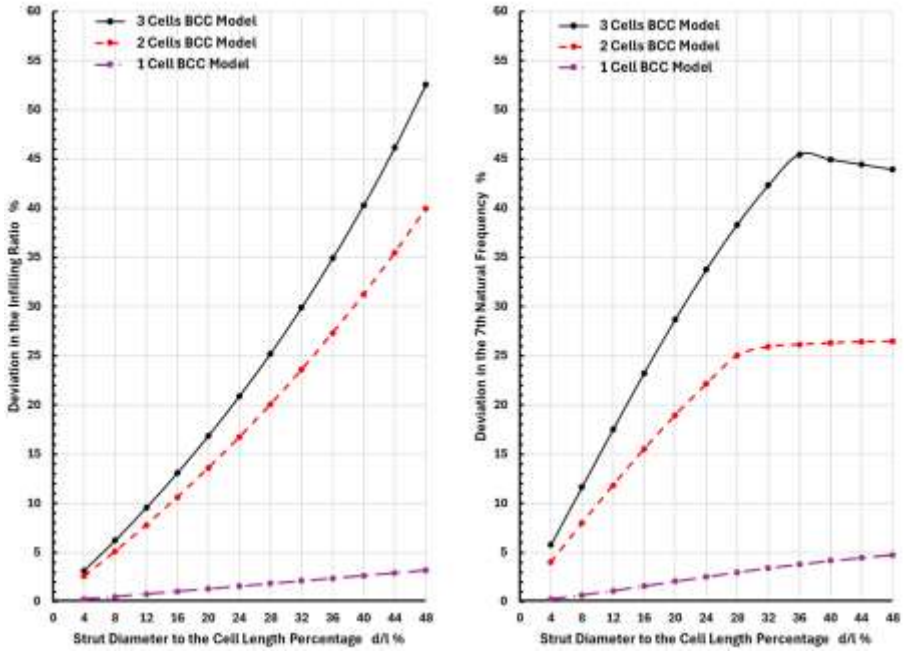

FIG. 7. DEVIATION IN FREQUENCY AND FILLING RATIO BETWEEN BEAM AND SOLID MODELS FOR 1X1, 2X2, AND 3X3 BCC CELL

IV. DISCUSSIONS

The discussion focuses on three intertwined aspects: geometric scaling, joint representation, and topology-dependent dynamic response. When the diameter-to-length ratio is held constant, scaling the cell size changes mass and stiffness in a self-similar manner, with mass scaling as x^3 and stiffness scaling approximately linearly with x, leading to natural frequencies scaling as 1/x. The simulations confirm this similarity: for a given topology and d/L%, the frequency of a 1 mm cell is approximately three times that of a 3 mm cell, and mode shapes remain unchanged. Consequently, the dominant geometric parameter controlling dynamic behaviour is not the absolute cell size, but the slenderness ratio, which governs bending stiffness via $EI \propto d^4$ and switches the structural response between strongly bending-dominated and more bulk-like regimes.

The comparison between beam and solid models reveals that the major source of discrepancy is not only stiffness modelling, but also the representation of mass and volume at joints. Beam elements treat joints as point connections and sum strut volumes independently, ignoring the finite overlapping and merging of solid struts. Solid models, by contrast, inherently redistribute material around intersections. As d/L% increases, joint regions occupy a larger fraction of the total volume, and mass aggregation around nodes becomes dominant. This leads beam models to overestimate relative density and infill ratio, especially in highly connected topologies where the number of intersecting struts and their combinatorial overlap grow rapidly. The strong correlation between infill ratio deviation and frequency deviation indicates that mass and stiffness are both misrepresented in beam formulations once the joint regions become non-negligible.

Topology plays a critical role in determining the magnitude and evolution of these discrepancies. BCC, with its limited number of joints and relatively simple connectivity, maintains low errors in both natural frequency and infill ratio across the full d/L% range. SC and AFCC, which add corner and face joints, exhibit progressively higher deviations; AFCC, in particular, shows up to 45% frequency deviation and a large overestimation of infill due to its higher joint count and more complex intersection patterns. Iso-Truss further increases joint complexity, with a central 14-strut intersection, and reaches infill predictions that exceed 100%, highlighting the inability of beam models to maintain physical realism at high d/L%. Octet-Truss and FBCCXYZ, with the highest joint densities, transition at relatively modest d/L% (≈36% and ≈24%, respectively) from a discrete lattice to an effectively bulk-like solid with residual voids. In this regime, beam models predict infill ratios up to 144–200% and large, though eventually saturating, frequency deviations, clearly indicating model breakdown.

The mesh sensitivity analysis supports these conclusions by showing that solid element convergence is more sensitive to slenderness than to cell size. As members become more slender, bending-dominated modes are increasingly mesh-dependent, necessitating sufficient circumferential and axial refinement to capture curvature and stress gradients. The optimum circumferential division (≈14–16 elements around the strut) provides an acceptable compromise between accuracy and computational cost, while still resolving local joint geometry. This finding is important because it emphasizes that accurate solid modelling of high-slenderness lattices is achievable with practical computational resources, particularly when compared with the large, topology-dependent errors observed in beam-only models at higher d/L%.

Extension to multi-cell configurations further emphasizes the cumulative impact of joints. For BCC, although the single-cell beam model deviates modestly, assembling 2×2 and 3×3 arrays dramatically increases the number of joints (to 120 and 424) and correspondingly amplifies both infill and frequency

International Journal of Engineering Research & Technology (IJERT)
ISSN: 2278-0181
Vol. 15 Issue 04 , April - 2026

deviations. Frequency errors grow from around 5% in a single cell to over 40% in the 3×3 configuration, and infill ratio deviations increase from ≈3% to beyond 50% at the same d/L%. This scaling with joint count indicates that even topologies that appear "beam-friendly" at the unit-cell level become progressively misrepresented as the structure size and connectivity grow. Consequently, the reliability of pure beam models in large lattice assemblies is much more limited than single-cell analyses suggest.

Overall, the results show that deviations between beam and solid models are controlled by three coupled parameters: d/L%, joint connectivity/complexity, and the effective transition from discrete lattice to bulk-like behaviour. Beam models perform well at low d/L% and low-to-moderate joint densities, where joint volumes are small and bending-dominated behaviour is well captured by Timoshenko formulations. As d/L% and joint complexity increase, the underlying assumptions of beam theory—slender members, negligible joint volume, and clear separation between member and node regions—are progressively violated, leading to non-physical infill predictions and large errors in natural frequencies and mode shapes. This behaviour motivates hybrid strategies that combine beam elements for slender spans with localized solid representations at joints or in highly congested regions, thus restoring mass and stiffness fidelity while avoiding the full computational cost of a purely solid model.

V. CONCLUSION

The conclusions drawn from this work establish explicit, topology-aware guidelines for modelling strut-based lattices under dynamic loads. First, the diameter-to-length ratio is the primary geometric parameter governing both dynamic response and modelling error. When d/L% is small, beam models provide accurate frequencies and reasonable infill predictions irrespective of cell size, because mass and stiffness scale similarly and joint volumes remain negligible. In this regime, beam-only modelling is appropriate and offers substantial computational savings.

Second, joint number and geometric complexity are the main drivers of divergence between beam and solid representations. As the number of intersecting struts per joint and the total joint count increase, beam models systematically overestimate volume and mass and misrepresent the stiffness distribution, particularly at higher d/L%. This effect is modest for low-connectivity topologies such as BCC, grows markedly for SC and AFCC, and becomes severe for Iso-Truss, Octet-Truss, and FBCCXYZ. For highly connected lattices, beam predictions of infill ratio can exceed 100–200%, and frequency deviations can surpass 40–50%, even for single cells, making pure beam models unsuitable for reliable dynamic design.

Third, cell size itself does not alter the fundamental deformation mode, provided d/L% is constant; instead, it produces predictable frequency scaling ($f \propto 1/x$) that is well captured by both beam and solid models. Therefore, model selection should be based primarily on slenderness and topology rather than absolute dimensions.

Fourth, mesh sensitivity studies confirm that accurately capturing bending-dominated behaviour and joint effects with solid elements is feasible with quadratic tetrahedra and moderate circumferential refinement, and that slenderness exerts a stronger influence on convergence than cell size. This supports the use of solid or locally refined solid regions in critical areas without prohibitive computational cost.

Finally, the accumulation of joints in multi-cell assemblies significantly amplifies the discrepancies observed at the unit-cell level. Even topologies that appear well represented by beams as single cells, such as BCC, exhibit rapidly increasing deviations in infill and frequency when scaled to 2×2 or 3×3 arrays. For large, highly connected lattices used in dynamic and impact applications, a hybrid modelling strategy emerges as the most robust approach: beam elements are employed for slender, low-congestion members, while solid elements are used at joints and in dense regions to restore correct mass and stiffness representation. These findings provide a quantitative framework for selecting and combining beam, solid, and hybrid models in a topology- and d/L%-dependent manner, enabling more reliable prediction of dynamic performance in practical lattice-based structures.

VI. CREDIT AUTHORSHIP CONTRIBUTION STATEMENT

Abdulrahman Ibrahim: Writing - review & editing, Conceptualization, Methodology, Software, Validation, Formal analysis, Investigation, Data curation, Writing - original draft, Visualization.

Khaled Ahmed: Project administration: Conceptualization, Methodology, Software, Validation, Formal analysis, Writing - review & editing.

Mahmoud Alzahrani: Resources, editing, Project administration, and Funding acquisition.

VII. DECLARATION OF COMPETING INTEREST

The authors declare that they have no known competing financial interests or personal relationships that could have appeared to influence the work reported in this paper.

VIII. ACKNOWEDGMENTS

The authors thank Strategic System Trading Co. Ltd. (STIRA), Jeddah, for providing access to their ANSYS workstation that is equipped with an AMD Ryzen Threadripper PRO 3995WX 64-core processor (4.0 GHz) with 256 GB RAM and for the use of their ANSYS license No. 1151820 to perform all numerical simulations reported in this article.

IX. REFERENCES

[1] G. Eason, B. Noble, and I.N. Sneddon, "On certain integrals of Lipschitz-Hankel type involving products of Bessel functions," Phil. Trans. Roy. Soc. London, vol. A247, pp. 529-551, April 1955. (*references*)

[2] Gibson LJ, Ashby MF. Cellular Solids: Structure and Properties. Cambridge Solid State Science Series. Cambridge University Press; 1997.

[3] Ashby, M.F. (2005) 'The properties of foams and lattices', Philosophical Transactions of the Royal Society A: Mathematical, Physical and

Engineering Sciences, 364(1838), pp. 15–30. doi:10.1098/rsta.2005.1678.

[4] ANSYS, Inc. (2024). Line Bodies (ANSYS Workbench Mechanical Documentation, Release 2024 R2). ANSYS Help.

[5] Ewins, D.J. (2000) Modal testing: Theory, practice and application. 2nd edn. Baldock: Research Studies Press.

[6] Öchsner, A. (2021). Timoshenko Beam Theory. In: Classical Beam Theories of Structural Mechanics. Springer, Cham. doi.org/10.1007/978-3-030-76035-9_3

[7] Alomar, Z. and Concli, F. (2021) 'Numerical modeling of selective laser melting lattice structures: A review of approaches', IOP Conference Series: Materials Science and Engineering, 1038(1), p. 012002. doi:10.1088/1757-899x/1038/1/012002.

[8] Tahmasebimoradi, A., Mang, C. and Lorang, X., 2021, November. A numerical hybrid finite element model for lattice structures using 3d/beam elements. In ASME International Mechanical Engineering Congress and Exposition (Vol. 85550, p. V02AT02A061). American Society of Mechanical Engineers.

[9] Carlton, H.D., Volkoff-Shoemaker, N.A., Messner, M.C., Barton, N.R. and Kumar, M., 2022. Incorporating defects into model predictions of metal lattice-structured materials. Materials Science and Engineering: A, 832, p.142427.

[10] Amir, E. and Amir, O., 2019. Topology optimization for the computationally poor: efficient high resolution procedures using beam modeling. Structural and Multidisciplinary Optimization, 59(1), pp.165-184.

[11] Schasching, M.M., Červinek, O., Koutný, D., Pettermann, H.E. and Todt, M., 2025. A Uniaxial Hysteretic Superelastic Constitutive Model Applied to Additive Manufactured Lattices. PAMM, 25(1), p.e202400092.

[12] Zhong, H., Song, T., Li, C., Das, R., Gu, J. and Qian, M., 2023. The Gibson-Ashby model for additively manufactured metal lattice materials: Its theoretical basis, limitations and new insights from remedies. Current Opinion in Solid State and Materials Science, 27(3), p.101081.

[13] Ushijima, K. et al. (2010) 'An investigation into the compressive properties of stainless steel micro-lattice structures', Journal of Sandwich Structures & Materials, 13(3), pp. 303–329. doi:10.1177/1099636210380997.

[14] Guadagnuolo, M. and Faella, G., 2017, January. Comparative seismic response of masonry buildings modelled by beam and solid elements. In Proceedings of the 16th World Conference on Earthquake Engineering, 16WCEE, Santiago, Chile (pp. 9-13).

[15] Savio, G., Curtarello, A., Rosso, S., Meneghello, R. and Concheri, G., 2019. Homogenization driven design of lightweight structures for additive manufacturing. International Journal on Interactive Design and Manufacturing (IJIDeM), 13(1), pp.263-276.

[16] Abou-Ali, A.M., Lee, D.W. and Abu Al-Rub, R.K., 2022. On the effect of lattice topology on mechanical properties of SLS additively manufactured sheet-, ligament, and strut-based polymeric metamaterials. Polymers, 14(21), p.4583.

[17] Altamimi, S., Lee, D.W., Barsoum, I., Rowshan, R., Jasiuk, I.M. and Abu Al-Rub, R.K., 2022. On stiffness, strength, anisotropy, and buckling of 30 strut-based lattices with cubic crystal structures. Advanced Engineering Materials, 24(7), p.2101379.

[18] Rizvi, Z.H., Wuttke, F. and Sattari, A.S., 2018, August. Dynamic analysis by lattice element method simulation. In Proceedings of China-Europe Conference on Geotechnical Engineering: Volume 1 (pp. 405-409). Cham: Springer International Publishing.

[19] Dash, S. and Nordin, A., 2023. Towards realistic numerical modelling of thin strut-based 3D-printed structures. Proceedings of the Design Society, 3, pp.3591-3600.

[20] Kamranfard, M.R., Darijani, H. and Khademzadeh, S., 2024. Mechanical behavior of Ti6Al4V lattice structures; numerical and experimental analysis. Mechanics of Advanced Materials and Structures, 31(4), pp.735-748.

[21] Luxner, M.H., Stampfl, J. and Pettermann, H.E. (2005) 'Finite element modeling concepts and linear analyses of 3D regular open cell structures', Journal of Materials Science, 40(22), pp. 5859–5866. doi:10.1007/s10853-005-5020-y.

[22] Gümrük, R. and Mines, R.A.W. (2013) 'Compressive behaviour of stainless steel micro-lattice structures', International Journal of Mechanical Sciences, 68, pp. 125–139. doi:10.1016/j.ijmecsci.2013.01.006.

[23] Chua, C., Sing, S.L. and Chua, C.K. (2022) 'Finite element analysis on titanium-tantalum lattice structures fabricated using selective laser melting', Materials Today: Proceedings, 70, pp. 616–621. doi:10.1016/j.matpr.2022.09.619.

[24] Maconachie, T. et al. (2021) 'The effect of topology on the quasi-static and dynamic behaviour of SLM AlSi10Mg lattice structures', The International Journal of Advanced Manufacturing Technology, 118(11–12), pp. 4085–4104. doi:10.1007/s00170-021-08203-y.

[25] Wang, P., Yang, F. and Zhao, J. (2022) 'Compression behaviors and mechanical properties of modified face-centered cubic lattice structures under quasi-static and high-speed loading', Materials, 15(5), p. 1949. doi:10.3390/ma15051949.

[26] Červinek, O. et al. (2021) 'Computational approaches of quasi-static compression loading of SS316L lattice structures made by selective laser melting', Materials, 14(9), p. 2462. doi:10.3390/ma14092462.

[27] Ruiz de Galarreta, S., Jeffers, J.R.T. and Ghouse, S. (2020) 'A validated finite element analysis procedure for porous structures', Materials & Design, 189, p. 108546. doi:10.1016/j.matdes.2020.108546.

[28] Smith, M., Guan, Z. and Cantwell, W.J. (2013) 'Finite element modelling of the compressive response of lattice structures manufactured using the selective laser melting technique', International Journal of Mechanical Sciences, 67, pp. 28–41. doi:10.1016/j.ijmecsci.2012.12.004.

[29] De Weer, T. et al. (2022) 'The parametrized superelement approach for lattice joint modelling and Simulation', Computational Mechanics, 70(2), pp. 451–475. doi:10.1007/s00466-022-02176-9.

[30] Park, K.-M., Min, K.-S. and Roh, Y.-S. (2021) 'Design optimization of lattice structures under compression: Study of unit cell types and cell arrangements', Materials, 15(1), p. 97. doi:10.3390/ma15010097.

[31] Di Caprio, F. et al. (2022) 'Ti-6Al-4V octet-truss lattice structures under bending load conditions: Numerical and experimental results', Metals, 12(3), p. 410. doi:10.3390/met12030410.

[32] Fang, N. et al. (2025) 'A dual mortar contact method for embedding 1D components into 3D geomaterials', Computers and Geotechnics, 186, p. 107339. doi:10.1016/j.compgeo.2025.107339.

[33] Shafqat, A., Weeger, O. and Xu, B.-X. (2024) 'A robust finite strain isogeometric solid-beam element', Computer Methods in Applied Mechanics and Engineering, 426, p. 116993. doi:10.1016/j.cma.2024.116993.

[34] White, D.A. et al. (2023) 'A reduced order model approach for finite element analysis of cellular structures', Finite Elements in Analysis and Design, 214, p. 103855. doi:10.1016/j.finel.2022.103855.

[35] Dong, G., Tang, Y. and Zhao, Y.F. (2017) 'Simulation of elastic properties of solid-lattice hybrid structures fabricated by additive manufacturing', Procedia Manufacturing, 10, pp. 760–770. doi:10.1016/j.promfg.2017.07.072.

[36] Cadart, T. et al. (2025) 'An optimal penalty method for the joint stiffening in beam models of additively manufactured lattice structures', International Journal of Solids and Structures, 306, p. 113107. doi:10.1016/j.ijsolstr.2024.113107.

[37] Dong, G. and Zhao, Y.F. (2018) 'Numerical and experimental investigation of the joint stiffness in lattice structures fabricated by additive manufacturing', International Journal of Mechanical Sciences, 148, pp. 475–485. doi:10.1016/j.ijmecsci.2018.09.014.

[38] Gholibeygi, S., Ergün, H. and Ayhan, B. (2025) 'Beam finite element model modification considering shear stiffness: Octet-truss unit cell with springs', Applied Sciences, 15(16), p. 8969. doi:10.3390/app15168969.

[39] Danesh, H. et al. (2025) 'A two-scale computational homogenization approach for elastoplastic truss-based lattice structures', Results in Engineering, 25, p. 103976. doi:10.1016/j.rineng.2025.103976.

[40] Klarmann, S., Wackerfuß, J. and Klinkel, S. (2022) 'Coupling 2d Continuum and beam elements: A mixed formulation for avoiding spurious stresses', Computational Mechanics, 70(6), pp. 1145–1166. doi:10.1007/s00466-022-02221-7.

[41] Steinbrecher, I. et al. (2020) 'A mortar-type finite element approach for embedding 1D beams into 3D solid volumes', Computational Mechanics, 66(6), pp. 1377–1398. doi:10.1007/s00466-020-01907-0.

[42] Jeong, H.S., Lyu, S.-K. and Park, S.H. (2021) 'Effective strut-based design approach of multi-shaped lattices using equivalent material properties', Journal of Mechanical Science and Technology, 35(4), pp. 1609–1622. doi:10.1007/s12206-021-0324-7.

International Journal of Engineering Research & Technology (IJERT)
ISSN: 2278-0181
Vol. 15 Issue 04 , April - 2026

[43] Perez-Garcia, C. et al. (2022) 'Beam formulation and FE framework for architected structures under finite deformations', European Journal of Mechanics - A/Solids, 96, p. 104706. doi:10.1016/j.euromechsol.2022.104706.

[44] Dash, J. et al. (2024) 'A hybrid continuum-beam optimisation model: The virtual extensometer method for efficient optimisation of lattice materials', Progress in Additive Manufacturing, 10(4), pp. 2535–2557. doi:10.1007/s40964-024-00766-y.

[45] Quevedo González, F.J. and Nuño, N. (2015) 'Finite element modelling approaches for well-ordered porous metallic materials for orthopaedic applications: Cost effectiveness and geometrical considerations', Computer Methods in Biomechanics and Biomedical Engineering, 19(8), pp. 845–854. doi:10.1080/10255842.2015.1075009.

[46] Grünfelder, N. et al. (2025) 'Reduced-order modeling of lattice structures through iterative beam fitting and static mesoscale projection', Results in Engineering, 27, p. 106529. doi:10.1016/j.rineng.2025.106529.

[47] Syam, W.P. et al. (2018) 'Design and analysis of strut-based lattice structures for vibration isolation', Precision Engineering, 52, pp. 494–506. doi:10.1016/j.precisioneng.2017.09.010.

[48] Wei, Y. et al. (2020) 'Damping behaviors of steel-based Kelvin lattice structures fabricated by indirect additive manufacture combining investment casting', Smart Materials and Structures, 29(5), p. 055001. doi:10.1088/1361-665x/ab78b8.

[49] Hussain, S. et al. (2022) 'Experimental and numerical vibration analysis of octet-truss-lattice-based gas turbine blades', Metals, 12(2), p. 340. doi:10.3390/met12020340.

[50] Kim, S.W., Kwon, Y.N. and Kang, B.S. (2012b) 'Influence of mesh density and element type on the accuracy of Fe analysis of periodic cellular structures', Advanced Materials Research, 445, pp. 583–588. doi:10.4028/www.scientific.net/amr.445.583.

[51] Liović, D. et al. (2024) 'A study on the compressive behavior of additively manufactured alsi10mg lattice structures', Materials, 17(21), p. 5188. doi:10.3390/ma17215188.

[52] Benedetti, M. et al. (2021) 'Architected Cellular Materials: A review on their mechanical properties towards fatigue-tolerant design and fabrication', Materials Science and Engineering: R: Reports, 144, p. 100606. doi:10.1016/j.mser.2021.100606.

[53] Bobbert, F.S.L. et al. (2017) 'Additively manufactured metallic porous biomaterials based on minimal surfaces: A unique combination of topological, mechanical, and mass transport properties', Acta Biomaterialia, 53, pp. 572–584. doi:10.1016/j.actbio.2017.02.024.

[54] ANSYS, Inc. (2021) ANSYS mechanical APDL theory reference. Release 2021 R1. Canonsburg, PA: ANSYS, Inc.

[55] Cook, R.D., Malkus, D.S., Plesha, M.E. and Witt, R.J. (2002) Concepts and applications of finite element analysis. 4th edn. New York: John Wiley & Sons.

[56] Zienkiewicz, O.C. and Taylor, R.L. (2000) The Finite Element Method. 5th edn. Oxford: Butterworth-Heinemann.

[57] ANSYS, Inc. (2021) ANSYS mechanical user's guide. Release 2021 R1. Canonsburg, PA: ANSYS, Inc.

[58] ANSYS, Inc. (2021) ANSYS mechanical APDL element reference. Release 2021 R1. Canonsburg, PA: ANSYS, Inc.

[59] Zienkiewicz, O.C. and Taylor, R.L. (2002) *The Finite Element Method Vol. 1 the basis O.C. Zienkiewicz; R.L. Taylor*. Oxford u.a.: Butterworth-Heinemann.

[60] Beer, F.P., Johnston, E.R., DeWolf, J.T. and Mazurek, D.F. (2012) Mechanics of Materials. 7th edn. New York: McGraw-Hill.

[61] Zeinali, Y. and Story, B. (2017) 'Framework for flexural rigidity estimation in Euler-Bernoulli beams using deformation influence lines', Infrastructures, 2(4), p. 23. doi:10.3390/infrastructures2040023.

[62] Young, W.C. and Budynas, R.G. (2002) Roark's formulas for stress and strain, Seventh edition. McGraw-Hill.